Article type: Original paper

Hand-held, clinical dual mode ultrasound - photoacoustic imaging of rat urinary bladder and its applications

*Kathyayini Sivasubramanian, Vijitha Periyasamy, Rhonnie Austria Dienzo, and Manojit Pramanik**

*Corresponding Author: E-mail: manojit@ntu.edu.sg, Phone: +6567905835, Fax: +65 67911761

School of Chemical and Biomedical Engineering, Nanyang Technological University, 62 Nanyang drive, Singapore 637459

Keywords: (Photoacoustic cystography, clinical photoacoustic imaging, handheld imaging, vesicoureteral reflux, clearance study)

Urinary bladder imaging is critical to diagnose urinary tract disorders, and bladder cancer. There is a great need for safe, non-invasive, and sensitive imaging technique which enables bladder imaging. Photoacoustic imaging is a rapidly growing imaging technique for various biological applications. It can be combined with clinical ultrasound imaging system for hand-held, dual modal ultrasound-photoacoustic real-time imaging. Structural (bladder wall) and functional (accretion of nanoparticles) bladder imaging is shown here with combined ultrasound and photoacoustic imaging in rats. Photoacoustic images of bladder wall is shown using black ink as the contrast agent. Chicken tissues were stacked on the abdomen of the animal to demonstrate the feasibility of photoacoustic imaging till a depth of 2 cm. Also, the feasibility of photoacoustic imaging for a common bladder disorder, vesicoureteral reflux is studied using urinary tract mimicking phantom. It is also shown that a clinical ultrasound system can be used for photoacoustic imaging of non-invasive clearance study of gold nanorods from circulation by monitoring the gradual accumulation of the gold nanorods in the bladder. The time taken for accumulation of nanorods in the bladder can be used as an indicator of the clearance rate of the nanoparticle circulation from the body.

1. Introduction:

Urinary bladder imaging is essential to monitor disorders such as urinary incontinence vesicoureteral reflux, cystitis, glomerulation, bladder cancer [1-3]. Severity of the diseases varies from causing minor discomfort to being fatal. Urinary incontinence is a condition when the person suffers from involuntary leakage of urine from the bladder. It can occur due to loss of control or failed sphincter muscle. This problem usually occurs due to aging. Vesicoureteral reflux (VUR) is the reverse flow of urine from the bladder to the kidney through the ureters. Urine usually flows from the kidney to the bladder through the ureters. The sphincter valve present at the junction of the ureters and bladder prevents the reverse flow. When reflux occurs, bacteria present in the bladder moves to the kidney causing further infection, scarring etc. The reflux occurs while voiding urine or at rest [4]. Cystitis is the bacterial infection of the urinary bladder [5]. If not treated on time, cystitis can lead to further complications. Glomerulation is another bladder disorder which is caused by haemorrhages [6]. Glomerulation and cystitis are highly related. While most of the urinary tract infections occur more commonly in women, bladder cancer occurs more frequently in men. The cancer begins on the wall of the bladder and eventually spreads, which is fatal to the patient. Therefore, imaging the urinary tract (ureter, bladder and urethra) is very important for early diagnosis [1, 7].

Some of the common clinical bladder imaging techniques include cystography, cystourethroscopy, ultrasound imaging and, optical imaging. Cystography is the gold standard for bladder imaging to evaluate bladder cancer, VUR, bladder polyps, hydronephrosis (inflammation of kidney due to water retention), etc. In cystography, a radio opaque contrast is injected into the bladder using urinary catheter and X-ray images of the bladder are obtained before, during, and after voiding to diagnose bladder related diseases [8, 9]. The sensitivity of the technique is not very high and injection of contrast agents increases the discomfort of the

patient [10]. Hence, there is a necessity for using safer and more sensitive imaging techniques to image the urinary tract.

Cystourethroscopy (CUSC) is another commonly used imaging modality to diagnose and follow-up on the urinary bladder wall and the urethra. This technique needs to be performed with local anaesthesia. A cystoscope (device similar to endoscope) is slowly inserted through the urethra as the camera gathers images of the bladder and the urethra. It is commonly used for imaging bladder lesions, cystitis, bladder cancer etc. CUSC has limited imaging depth and cannot provide 3-dimensional structural information of bladder wall [11]. Also, the image resolution is not the best.

Ultrasound (US) imaging is used for bladder imaging very frequently. US imaging allow higher imaging depths compared to CUSC, and are used to image the lower urinary system in women to detect genuine stress urinary incontinence. Additionally, US imaging also gives information of bladder wall lesion and bladder cancer [12]. The US imaging proved to be an efficient tool for Burch colposuspension [13-15]. 2D and 3D imaging of urinary bladder was compared. The mean error in measurement of urinary bladder dimensions in 3D imaging is 4.9% while the mean error was 27.5% in 2D ultrasound imaging. First febrile urinary tract infection in young children is detected using US imaging [16, 17].

Optical imaging such as multiphoton microscopy, fluorescence was used to study urinary bladder [18-20]. Computational model of urinary bladder was developed to study the propagation of ultraviolet and blue wavelength [21]. This model was used for differentiation of healthy and diseased urinary bladder using fluorescence imaging. Absorption and scattering

properties of porcine urinary bladder was studied from 400 nm to 1800 nm. Optical coherence tomography was used to differentiate inflammation, hyperplasia and neoplasia [22].

The different imaging techniques currently used for bladder imaging have several limitations including use of ionising radiation, invasive imaging, shallow imaging depth, poor resolution, and inadequate sensitivity. Therefore, a non-invasive, safe and better imaging alternative is required. Photoacoustic imaging (PAI) is a rapidly growing imaging technique. It combines the rich optical contrast with high ultrasound resolution [23-27]. It can be easily combined with other imaging techniques like ultrasound imaging, and fluorescence imaging to facilitate multimodal imaging. PAI is being explored as an alternative for bladder imaging due to its non-invasive and non-ionizing nature [28]. PAI uses a pulsed laser as the excitation source; upon absorption of light by the tissue chromophores, there occurs a small temperature rise. This temperature rise causes thermoelastic expansion, which generates pressure waves. The pressure waves are then detected with an ultrasound transducer and images are formed by reconstructing the data. PAI uses intrinsic contrast within the body (blood, melanin, water etc.) or uses extrinsic contrast agents like organic dyes and nanoparticles [29-35]. For bladder imaging there is no intrinsic contrast provided by the urine, therefore extrinsic contrast agents are needed. Dyes like methylene blue and indocyanine green (ICG) have been used for bladder imaging [36]. For non-invasive monitoring of vesicoureteral reflux, ICG enhanced carbon nanotubes are injected into the rats and monitored over time [37]. PAI of canine urinary bladder was studied to determine the presence of muscularis propia invasion. Murine urinary bladders were imaged for oxygen saturation computation [38]. PA imaging was combined with fluorescent imaging for quantification of ICG accumulation in urinary bladder. Vasculature of urinary bladder is imaged using photoacoustic microscopy [39, 40].

These studies were done with laboratory prototype photoacoustic imaging systems which uses single element transducer for image acquisition, with very limited clinical translational capability. The first clinically compatible PA-US system reported more than a decade ago by Erpelding *et al.*, was not based on clinical ultrasound platform available commercially [41]. It was based on Philips iU22 ultrasound imaging system, with custom made modification to access the raw channel radio frequency (RF) data. These custom modifications cannot be done by any other external users. Therefore, such system cannot be replicated by any other research group/users. Only recently (last few years), commercial clinical ultrasound machines with access to raw channel data is made available. Availability of raw channel data is a must to acquire and reconstruct photoacoustic imaging. Thus, any research group/user now can purchase such ultrasound system and modify easily to incorporate photoacoustic imaging. Therefore, only recently it has become feasible for researcher to use clinical ultrasound and photoacoustic imaging together [42]. With these systems PAI can be easily translated to clinics for various applications. Clinical ultrasound systems with combined light delivery and image acquisition are being explored for various biological applications recently [42-45].

In this study, real-time photoacoustic imaging of urinary bladder was combined with ultrasound imaging to obtain structural and functional information. A clinical dual mode ultrasound and photoacoustic imaging system was used for bladder imaging for the first time. For deep tissue imaging, 1064 nm light was used as the photoacoustic excitation source. Contrast agent (black ink) was injected into the urinary bladder to show the structural PA imaging. Sagittal and transverse sections of urinary bladder were shown in PA and ultrasound modes up to a depth of 2 cm. The feasibility of using combined US and PA imaging was demonstrated for VUR in phantom imaging as modelling the disease in living rat is very challenging. Along with structural information PA imaging can also provide functional information, which was

demonstrated with combined US-PA imaging of nanoparticle clearance from the body. Nanoparticle clearance from the body was studied by injecting commercially available gold nanorods, through tail vein injection and tracking the accumulation of nanorods in the bladder at regular intervals over a time period of 150 minutes.

2. Materials and Methods:

2.1. US-PA imaging system:

For photoacoustic imaging, light from a frequency doubled nanosecond pulsed Nd:YAG pump laser (Continuum, Surelite Ex, San Jose, California, USA) was used. The pulse repetition frequency of the laser is 10 Hz and it produces pulses of 5 nanoseconds in duration. A dichroic mirror was used to transmit light at a wavelength of 1064 nm and reflect 532 nm. Light at 1064 nm was transmitted through the bifurcated optical fiber bundle (Ceramoptec GmbH, Germany). The fiber bundle contains 1600 optical fibers (core diameter of 185 μm and a numerical apertutre of 0.22) which were bifurcated in the middle to spread equally over two rectangles of area 4 cm X 0.1 cm. For image acquisition, a clinical research ultrasound system (E-CUBE 12R, Alpinion, South Korea) which can acquire photoacoustic and ultrasound images simultaneously was used. A clinically compatible linear array ultrasound transducer was used for data acquisition. The L3-12 linear array transducer has 128 elements with a center frequency of 8.5 MHz and 95% fractional bandwidth with an active area of 3.85 X 1 cm. The two rectangular fiber bundles and the linear array transducer were fitted into the designated slots of the custom fabricated (3D printed) probe holder to form the handheld probe. They were fixed in such a manner that the fiber to transducer distance was approximately 2 cm; the fiber to tissue distance was 1 cm and a light delivery angle of 15˚. Clear ultrasound gel was used for coupling [46]. **Figure 1** shows the schematic representation of the experimental set-up.

The clinical E-CUBE imaging system was operated in the combined US and PA mode (it can be operated separately as well). The acquired data can be saved in different formats including radiofrequency (RF), beam-formed, scan converted, or I.Q. data. This can be specified through programming in python script along with other parameters like imaging depth and total number of frames to be saved. The acquired images were saved as beam-formed data type for this study and an imaging depth of 3 cm was set for bladder imaging. Since the imaging system has only 64 parallel DAQ hardware, data can be collected only from 64 channels for every laser pulse. Data acquisition is initiated only when there was a trigger from the laser (directly from laser or through a photodiode) to the E-CUBE system. Hence, two laser pulses are required to collect data from all the 128 channels. The system combines the data obtained from the 128 channels (after two laser pulses) to form one single image (B-scan). Hence, the effective frame rate was 5 frames per second as the pulse repetition rate of the laser is 10 Hz.

2.2. Animal preparation:

Animal experiments were performed in accordance with the approved guidelines and regulations, and were approved by the Institutional Animal Care and Use Committee of Nanyang Technological University, Singapore (Animal Protocol Number ARF-SBS/NIE-A0263). Healthy adult male Sprague Dawley rats of weight 225±25 g (aged 8-10 weeks) were obtained from InVivos Pte. Ltd., Singapore. The rats were anesthetized using a mixture containing Ketamine and Xylazine of dosage of 85 and 15 mg/kg, respectively before experimentation. 0.2 mL of the mixture per 100 g of the rat body weight was administered by an intraperitoneal injection. Hair from the abdominal area of the rat was removed using commercial depilatory cream before imaging. A 23G urinary bladder catheter was inserted through the urethra and was secured with tissue glue to prevent leakage. During experiments, animal was maintained under anaesthesia with 0.75% of isoflurane gas (Medical Plus Pte Ltd,

Singapore) along with oxygen (1.2 L/min). The mixture was delivered through a nose cone wrapped with a breathing mask covering the mouth and nose of the animal completely. Heart rate and peripheral oxygen saturation of the animal was monitored continuously throughout the experiments using a pulse oximeter (Medtronic, PM10N with veterinary sensor, Minneapolis, Minnesota, USA). The animal was placed in supine position and images (US + PA) were recorded with the handheld probe. After image acquisition, the animal was euthanized with an overdose of pentobarbital.

2.3. Structural imaging of bladder:

A rectangular chicken tissue slice (7 X 6 cm) of approximately 1 cm in thickness was placed on the abdominal region of the rat. Black ink was used as the PA contrast agent and saline was used as control. Combined US and PA image of the bladder was taken before injection of dye or saline in both the transverse and the sagittal plane. 0.8 mL of black ink or saline was injected into the bladder through the catheter. After 10 minutes, the bladder was imaged in both the planes. Once, the PA signal from the bladder was clearly visible, depth imaging was performed. For depth imaging chicken tissue slices of 0.5 cm thickness was stacked one by one until a depth of 2 cm. Combined US and PA images were obtained and stored in both the transverse and sagittal plane.

2.4. Flow imaging:

Vesicoureteral reflux is a condition where there is a reverse flow of urine from the bladder to the kidney via the ureters. To demonstrate the feasibility of imaging the flow of urine from the bladder into the ureters, phantom imaging was done as modelling the disorder in rats is very difficult. A phantom was made with low-density polyethylene (LDPE) tubes of diameter 1.6 mm and latex material in ellipsoidal shape to mimic the urinary system. The tubes mimic the

urethra and the ureters; the latex material was made in the ellipsoidal shape to mimic the urinary bladder. The phantom was placed on a chicken tissue slice of thickness 3 cm and a 0.5 cm chicken tissue slice was placed on top. Combined US and PA imaging was done. The handheld probe was moved along the tissue slice to identify the ureter mimicking phantom with US imaging. The handheld probe was held in the same position. The bladder mimicking phantom was filled with black ink slowly through the urethral phantom. Slowly the black ink flows through the ureter phantom. A video showing the combined US ad PA imaging flow of the black ink from the bladder through the ureters was recorded from the screen.

2.5. Clearance imaging:

Combined US and PA imaging can be used for imaging nanoparticle clearance from the body. To demonstrate this 0.2 mL of gold nanorods (35μM/mL) (Sigma Aldrich, USA) of average size 10 nm was injected into the bloodstream of the rat through a tail vein injection. The gold nanorods have high optical absorption at 1064 nm therefore strong PA signal is expected. The bladder catheter was closed to prevent leakage through the urethra. A 1 cm thick chicken tissue was placed on the abdominal region for optimising light delivery. The bladder was imaged to obtain combined US and PA images in the sagittal and the transverse plane over a period of 150 minutes at regular intervals of 15 minutes [47]. The signal to noise ratio (SNR) was calculated from the saved PA images and plotted across time. For comparison an ellipsoidal phantom of 1.5 mL volume (roughly the size of a full bladder) containing 0.2 mL of gold nanorods was imaged and the SNR was calculated. For phantom imaging the phantom was placed on top of a 3 cm thick chicken tissue slice and covered with a 1 cm thick chicken tissue slice to mimic the *in vivo* imaging condition. The SNR value from the phantom imaging can be compared with the SNR calculated from the *in vivo* bladder data to determine the rate of clearance of gold nanorods from circulation.

2.6. Laser safety:

The coupling efficiency of the fiber bundle at 1064 nm was ~50%. The energy of light falling on the surface was ~45 mJ per pulse. The total area of illumination was ~5 cm^2 [46]. Therefore, the fluence can be calculated approximately as 9 mJ/cm^2 on the surface (skin). The maximum permissible energy (MPE) on skin at 1064 nm is 100 mJ/cm^2 according to the American National Standards Institute (ANSI) [48]. Therefore, all studies were done well within the prescribed safety limit.

3. Results and discussions:

Non-invasive imaging of urinary bladder (UB) is very useful for different applications. Here, we show the structural imaging of the UB with combined US and PA imaging. Additionally, PA imaging of back flow of the urine from the bladder to the kidney is shown with a bladder and ureter mimicking phantom for VUR imaging. Then, non-invasive imaging of clearance of nanoparticles (which has photoacoustic contrast) from the body through bladder is shown. For experiments, the rat bladder was imaged along the sagittal and transverse planes as shown in Figure 1.

Black ink was used as a photoacoustic contrast agent due to its strong absorbance at the near infrared wavelength window. For experiments, 1064 nm was chosen as the imaging wavelength. Due to weak absorption of light and lower scattering, the penetration depth of light is high at this wavelength. For urinary bladder imaging a high imaging depth is needed especially in human, as the abdominal muscle is of few centimetres thickness. Saline was used as control as it does not have any photoacoustic contrast at 1064 nm. **Figures 2(a) and 2(b)** show the combined US-PA image of the urinary bladder (before injection of saline) of the rat

in the sagittal and transverse plane, respectively. **Figures 2(c) and 2(d)** show the US-PA image of UB after injection of saline in the sagittal and transverse planes, respectively. It is to be noted from the images that there is no PA signal from the bladder both before and after injection of saline. However, from the ultrasound image the structure of the bladder can be clearly delineated and it can be noted that there is an increase in the size of the bladder after injection of saline through the catheter. **Figures 2(e) and 2(f)** show the sagittal and transverse combined US-PA images before injection of black ink. It can be observed that the bladder structure can be seen in US, but there is no PA signal from the bladder. **Figures 2(g) and 2(h)** show the combined US-PA images of the UB after injection of black ink through the catheter in the sagittal and transverse plane, respectively. After injection, there was a strong PA signal from the bladder wall from the black ink. The PA signal from the bladder is highlighted. In the images, the PA signal is visible from the top part of the bladder. The strong signal from the top surface masks the PA signal from the bottom part of the bladder. The grayscale image represents the US image and the colour is a representative of PA signal. Structural information will help in identifying bladder wall deformity, which can indicate bladder disorders.

In rats the bladder is located very close to the skin. In humans, the bladder is located much deeper depending on the muscular and fat content of the person, typically 2-3 cm. Therefore, combined US-PA imaging of bladder at different depths (using chicken tissue) is shown in both sagittal and transverse planes. **Figures 3(a-d)** show combined US-PA images of the bladder at different depths of 0.5 cm, 1 cm, 1.5 cm, and 2 cm in the sagittal plane. **Figures 3(e-h)** show the combined US-PA images of the rat urinary bladder in the transverse plane at different depths (0.5 cm, 1 cm, 1.5 cm, and 2 cm). From the images it can be observed that the PA signal is very prominent when the imaging depth is 0.5 cm and 1 cm. After 1 cm, the PA signal decreases with increase in depth. However, there is significant PA signal for imaging the

bladder even at higher depths. It is also important to note the fluence of imaging is much lesser than MPE advised by ANSI for 1064 nm. Therefore, the imaging depth can be improved further by increasing the laser power, thereby increasing the fluence or by using extrinsic contrast agent with higher light absorption at 1064 nm.

From the saved beam-formed images, SNR of the PA signal from the bladder was calculated at different depths. SNR is given by $SNR = 20 * \log_{10}(V/n)\ (dB)$, where V is the PA signal amplitude and n is the standard deviation of the background noise. 30 frames were averaged and the SNR was calculated from the averaged image. The calculated SNR was plotted against depth of imaging as shown in **Figure 3(i)**. It can be noted from the plot that the maximum SNR is at 1 cm depth, which is expected, as the illumination angle of 15˚ works best at 1 cm [43, 46]. Even at 2 cm imaging depth the SNR value is approximately 32 dB, which is sufficiently high for imaging. As stated earlier, since imaging was done at a very low energy, there is scope for getting higher SNR values at higher energy levels.

Vesicoureteral reflux is a very common urinary tract disease. Currently, this is imaged with the help of X-Ray cystography, during micturition and normal state. However, during X-ray imaging, the patient gets exposed to ionizing radiation. Therefore, PA imaging is a non-invasive and a safer imaging alternative for imaging and diagnosing vesicoureteral reflux. Urinary tract was modelled in phantom for imaging. **Figures 4(a-b)** show the ureter phantom images before and after the back flow from the urinary bladder. US imaging was used for locating the ureter phantom. The backflow is also shown in **Movie 1** which shows the black ink flowing through the ureters from the bladder. In rats the ureter diameter is very small, so phantom of 1 mm diameter was used for experiments. But in humans, the ureter can be easily located with ultrasound and vesicoureteral reflux can be imaged with PA imaging with a

suitable PA contrast agent under different conditions (before, during, and after bladder voiding) to determine when it occurs.

Another application for which PA imaging of bladder can be used is for monitoring clearance of nanoparticles from the body. There are not many non-invasive techniques to monitor clearance of contrast agent from the body. PA imaging can be used for clearance study if the nanoparticle provides a good photoacoustic signal (high optical absorption) at the specific wavelength. For this experiment commercially, available gold nanorods were introduced into blood through a tail vein injection and the bladder of the rat was continuously monitored for 150 min at 15 min interval in both sagittal and transverse planes. The SNR at different time points was calculated and plotted across time in **Figure 5(i)**. **Figures 5(a-d)** and **Figures 5(e-h)** show the combined US-PA image of the UB at different time intervals of 0 min, 15 min, 60 min, and 120 min in the sagittal and transverse planes, respectively. From **Figure 5(i)** it can be observed that the SNR keeps gradually increasing with time. Also from the images the PA signal increase can be observed. With increase in time the nanoparticles tend to settle down gradually and PA signal can be observed from the bottom wall of the bladder. A phantom with volume similar to a full bladder (1.5 mL) with 0.2 mL of gold nanorods was modelled, imaged and the SNR was calculated. The phantom imaging was mimicking the *in vivo* imaging scenario very closely. The SNR value was found to be 42 dB. The SNR calculated from the *in vivo* rat bladder images at the end of five hours was found to be 35 dB. Therefore, it can be roughly estimated that the average clearance time for ~50% gold nanorods from circulation is around 150 min. The rate of elimination depends on the enhanced permeation and retention properties of the nanoparticle. For different particles the clearance rate will vary.

In this work we have discussed about the different prospects of using clinical US-PA imaging system for urinary bladder imaging. PA imaging can be used for structural and functional imaging of the bladder. Imaging of vesicoureteral reflux (common bladder disorder) using PAI is focused. However, with the right contrast agents (targeted nanoparticle for bladder cancer); we believe PAI can be used extensively for bladder imaging and can aid in the diagnosis of bladder related disorders. However, there are some limitations with the current format of clinical PA imaging. One of the limitations is the fiber based light delivery; it limits the maximum light energy that can be transported to the transducer end. Therefore, this limits us from operating the system at the highest possible energy within the ANSI permissible limit. With higher laser energy better images can be obtained and also depth of imaging can also be improved. Hence, cost-effective fibres withstanding high energy is much needed for improved imaging. Another problem related to the optical fiber is that its flexibility determines the angle of light illumination, which affects the optimum imaging depth greatly. Therefore, it is important to have a very flexible fiber which allows different light illumination angles and use the optimum light illumination angle for the required depth of imaging. Another limitation for the current imaging system is its inability to provide good 3-D imaging. It is very difficult to have uniform hand motion at uniform time-intervals, therefore, the 3D imaging can be done only with a raster scan by motorised stage. A better 3D imaging platform may provide more information regarding the structure and function of the bladder.

4. Conclusion:

Combined ultrasound photoacoustic clinical imaging systems are being explored for different biological applications. Integration of handheld photoacoustic imaging together with ultrasound system currently used in clinic will support bedside monitoring. Even though PA imaging of urinary bladder has been discussed earlier, its feasibility through clinical ultrasound

system is shown here. Structural and functional urinary bladder imaging in small animals is demonstrated with the handheld combined ultrasound and photoacoustic imaging system. Up to 2 cm imaging depth is shown. Also, diagnosis of vesicoureteral reflux, a common bladder disorder, is demonstrated with phantom imaging. Additionally, functional PA imaging of clearance of nanoparticles from circulation is also demonstrated by monitoring the accumulation of gold nanorods in the bladder.

Supporting information

Additional supporting information may be found in the online version of this article at the publisher's website.

Movie S1: Movie showing the combined US and PA imaging of the back flow of the black ink in the ureter mimicking phantom.

Acknowledgements:

The authors would like to acknowledge the financial support from the Tier 1 research grant funded by the Ministry of Education in Singapore (RG48/16: M4011617) and Tier 2 research grant funded by Ministry of Education in Singapore (ARC2/15: M4020238). Authors have no relevant financial interests in this work and no other potential conflicts of interest to disclose.

Author biographies

Please see Supporting Information online.

References:

[1] S. Wu *Med. Ultrason.* **2013**, *15*, 161-163.

[2] W. M. L. L. G. Deserno, M. G. Harisinghani, M. Taupitz, G. J. Jager, J. A. Witjes, P. F. Mulders, C. A. Hulsbergen van de Kaa, D. Kaufmann, J. O. Barentsz *Radiology*. **2004**, *233*, 449-456.

[3] V. Kundra, P. M. Silverman *American Journal of Roentgenology*. **2003**, *180*, 1045-1054.

[4] Gabrielle Williams, Jeffery T. Fletcher, Stephen I. Alexander, J. C. Craig *J. Am. Soc. Nephrol.* **2008**, *19*, 847-862.

[5] G. Lee, R. Romih, D. ZupanIiI *BioMed Research International*. **2014**, *2014*, 10.

[6] Stephanya Shear, R. Mayer. *Urology*. **2006**, *68*, 253-256.

[7] M. C. Kriegmair, T. Bergen, M. Ritter, P. Mandel, M. S. Michel, T. Wittenberg, C. Bolenz *Urology*. **2017**, *104*, 235-241.

[8] Andrew J. Deck, Sarah Shaves, L. Talner, J. R. Porter *The Journal of Urology*. **2000**, *164*, 43-46.

[9] D. E. Morgan, L. K. Nallamala, P. J. Kenney, M. S. Mayo, L. W. Rue *American Journal of Roentgenology*. **2000**, *174*, 89-95.

[10] K. S. Han, H. J. Choi, D. C. Jung, S. Park, K. S. Cho, J. Y. Joung, H. K. Seo, J. Chung, K. H. Lee *Clin. Radiol.* **2011**, *66*, 251-256.

[11] M. Riccabona, T. R. Nelson, D. H. Pretorius, T. E. Davidson *J. Ultrasound Med.* **1996**, *15*, 627-632.

[12] C. H. Lee, C. H. Tan, S. d. C. Faria, V. Kundra *American Journal of Roentgenology*. **2017**, *208*, 1193-1205.

[13] V. Zutshi, B. Makkar, A. Garg, S. Batra *Journal of Clinical and Diagnostic Research : JCDR*. **2017**, *11*, QC01-QC03.

[14] V. Viereck, W. Bader, T. Krauß, M. Oppermann, A. Gauruder-Burmester, R. Hilgers, R. Hackenberg, W. Hatzmann, G. Emons *BJOG*. **2005**, *112*, 791-796.

[15] A. Martan, J. Mašata, M. Halaška, R. Voigt *Ultrasound Obstet. Gynecol.* **2001**, *17*, 58-64.

[16] A. Hoberman, M. Charron, R. W. Hickey, M. Baskin, D. H. Kearney, E. R. Wald *N. Engl. J. Med.* **2003**, *348*, 195-202.

[17] S. Mahant, J. Friedman, C. MacArthur *Arch. Dis. Child.* **2002**, *86*, 419.

[18] J. Hornsby, D. M. Daly, D. Grundy, F. Cheng, A. M. Robertson, P. N. Watton, M. S. Thompson *Acta biomaterialia*. **2017**.

[19] H. J. Lee, C. V. Barback, C. K. Hoh, Z. Qin, K. Kader, D. J. Hall, D. R. Vera, C. J. Kane *J. Nucl. Med.* **2017**, *58*, 547-553.

[20] B. E. Schaafsma, F. P. R. Verbeek, H. W. Elzevier, Q. R. J. G. Tummers, J. R. van der Vorst, J. V. Frangioni, C. J. H. van de Velde, R. C. M. Pelger, A. L. Vahrmeijer *J. Surg. Oncol.* **2014**, *110*, 845-850.

[21] I. E. Rafailov, V. V. Dremin, K. S. Litvinova, A. V. Dunaev, S. G. Sokolovski, E. U. Rafailov *J. Biomed. Opt.* **2016**, *21*, 025006.

[22] T. Q. Xie, M. L. Zeidel, Y. T. Pan *Opt. Express*. **2002**, *10*, 1431-1443.

[23] L. Li, L. Zhu, C. Ma, L. Lin, J. Yao, L. Wang, K. Maslov, R. Zhang, W. Chen, J. Shi *Nature Biomedical Engineering*. **2017**, *1*, 0071.

[24] P. Zhang, L. Li, L. Lin, P. Hu, J. Shi, Y. He, L. Zhu, Y. Zhou, L. V. Wang *Journal of biophotonics*. **2017**.

[25] P. K. Upputuri, M. Pramanik *J. Biomed. Opt.* **2017**, *22*, 041006.

[26] L. V. Wang, J. Yao *Nat Methods*. **2016**, *13*, 627-638.

[27] P. Beard *Interface Focus*. **2011**, *1*, 602-631.

[28] C. Kim, M. Jeon, L. V. Wang *Opt. Lett.* **2011**, *36*, 3599-3601.

[29] Y. Jiang, P. K. Upputuri, C. Xie, Y. Lyu, L. Zhang, Q. Xiong, M. Pramanik, K. Pu *Nano Lett.* **2017**, *17*, 4964-4969.

[30] Y. Gawale, N. Adarsh, S. K. Kalva, J. Joseph, M. Pramanik, D. Ramaiah, N. Sekar *Chemistry - A European Journal*. **2017**, *23*, 6570-6578.

[31] K. Sivasubramanian, M. Mathiyazhakan, C. Wiraja, P. K. Upputuri, C. Xu, M. Pramanik *J. Biomed. Opt.* **2017**, *22*, 041007.

[32] J. E. Lemaster, J. V. Jokerst *Wiley Interdiscip Rev Nanomed Nanobiotechnol*. **2017**, *9*.

[33] Y. Zhou, D. Wang, Y. Zhang, U. Chitgupi, J. Geng, Y. Wang, Y. Zhang, T. R. Cook, J. Xia, J. F. Lovell *Theranostics*. **2016**, *6*, 688-697.

[34] S. Huang, P. K. Upputuri, H. Liu, M. Pramanik, M. Wang *Journal of Materials Chemistry B*. **2016**, *4*, 1696-1703.

[35] C. Kim, C. Favazza, L. V. Wang *Chem. Rev.* **2010**, *110*, 2756-2782.

[36] S. Park, J. Kim, M. Jeon, J. Song, C. Kim *Sensors*. **2014**, *14*, 19660-19668.

[37] J. Koo, M. Jeon, Y. Oh, H. W. Kang, J. Kim, C. Kim, J. Oh *Phys. Med. Biol.* **2012**, *57*, 7853.

[38] C. Scheepbouwer, S. Meyer, M. J. Burggraaf, J. Jose, C. F. Molthoff *PLoS One*. **2016**, *11*, e0161284.

[39] A. Kamaya, S. Vaithilingam, B. I. Chung, O. Oralkan, B. T. Khuri-Yakub *J. Ultrasound Med.* **2013**, *32*, 1245-1250.

[40] Z. Xie, W. Roberts, P. Carson, X. Liu, C. Tao, X. Wang *Opt. Lett.* **2011**, *36*, 4815-4817.

[41] T. N. Erpelding, C. Kim, M. Pramanik, L. Jankovic, K. Maslov, Z. Guo, J. A. Margenthaler, M. D. Pashley, L. V. Wang *Radiology*. **2010**, *256*, 102-110.

[42] J. Kim, S. Park, Y. Jung, S. Chang, J. Park, Y. Zhang, J. F. Lovell, C. Kim *Sci. Rep.* **2016**, *6*, 35137.

[43] K. Sivasubramanian, V. Periyasamy, M. Pramanik *Journal of biophotonics*. **2018 (In Press)**.

[44] N. Gandhi, M. Allard, S. Kim, P. Kazanzides, M. A. L. Bell *J. Biomed. Opt.* **2017**, *22*, 121606.

[45] Y.-J. Lee, E.-J. Jeong, H.-W. Song, C.-G. Ahn, H. W. Noh, J. Y. Sim, D. H. Song, M. Y. Jeon, S. Lee, H. Kim *J. Biomed. Opt.* **2017**, *22*, 091513-091513.

[46] K. Sivasubramanian, V. Periyasamy, K. K. Wen, M. Pramanik *J. Biomed. Opt.* **2017**, *22*, 041008.

[47] Daniëlle PK Lankveld, Raja G Rayavarapu, Petra Krystek, Agnes G Oomen, Hennie W Verharen, Ton G van Leeuwen, Wim H De Jong, S. Manohar *Nanomedicine*. **2011**, *6*, 339-349.

[48] *American National Standard for Safe Use of Lasers*, ANSI Standard Z136.1-2007, American National Standards Institute, Inc., New York, NY. **2007**.

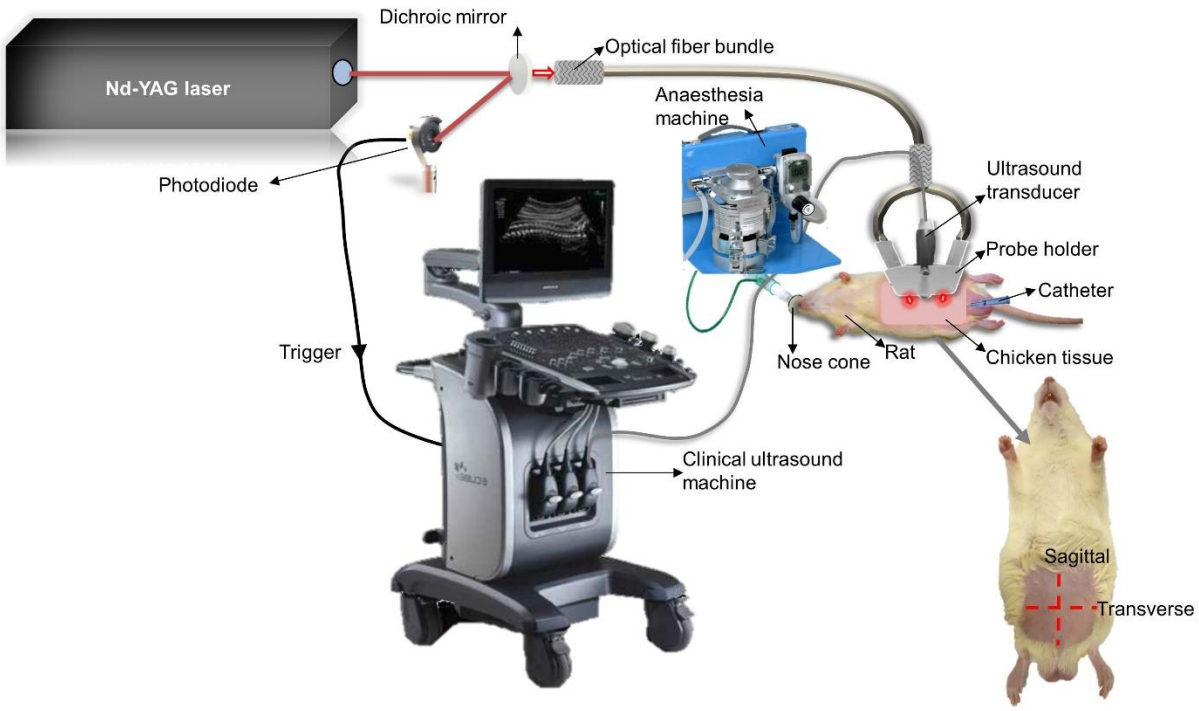

Figure 1. Schematic representation of the combined ultrasound-photoacoustic imaging system for *in vivo* imaging.

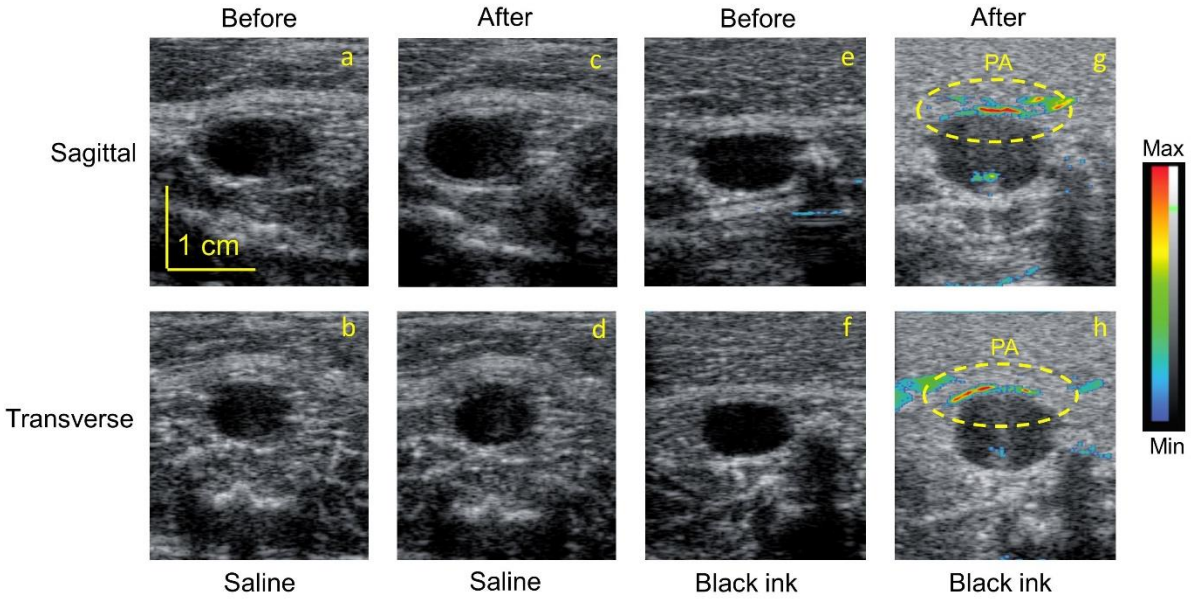

Figure 2. Structural imaging: (a-d) Sagittal plane imaging - (a,b) Combined US-PA image of the rat urinary bladder before and after injection of saline; (c,d) combined US-PA image of the rat bladder before and after injection of black ink. (e-h) Transverse plane imaging – (e,f) Combined US-PA image of the rat urinary bladder before and after injection of saline; (g,h) combined US-PA image of the rat bladder before and after injection of black ink.

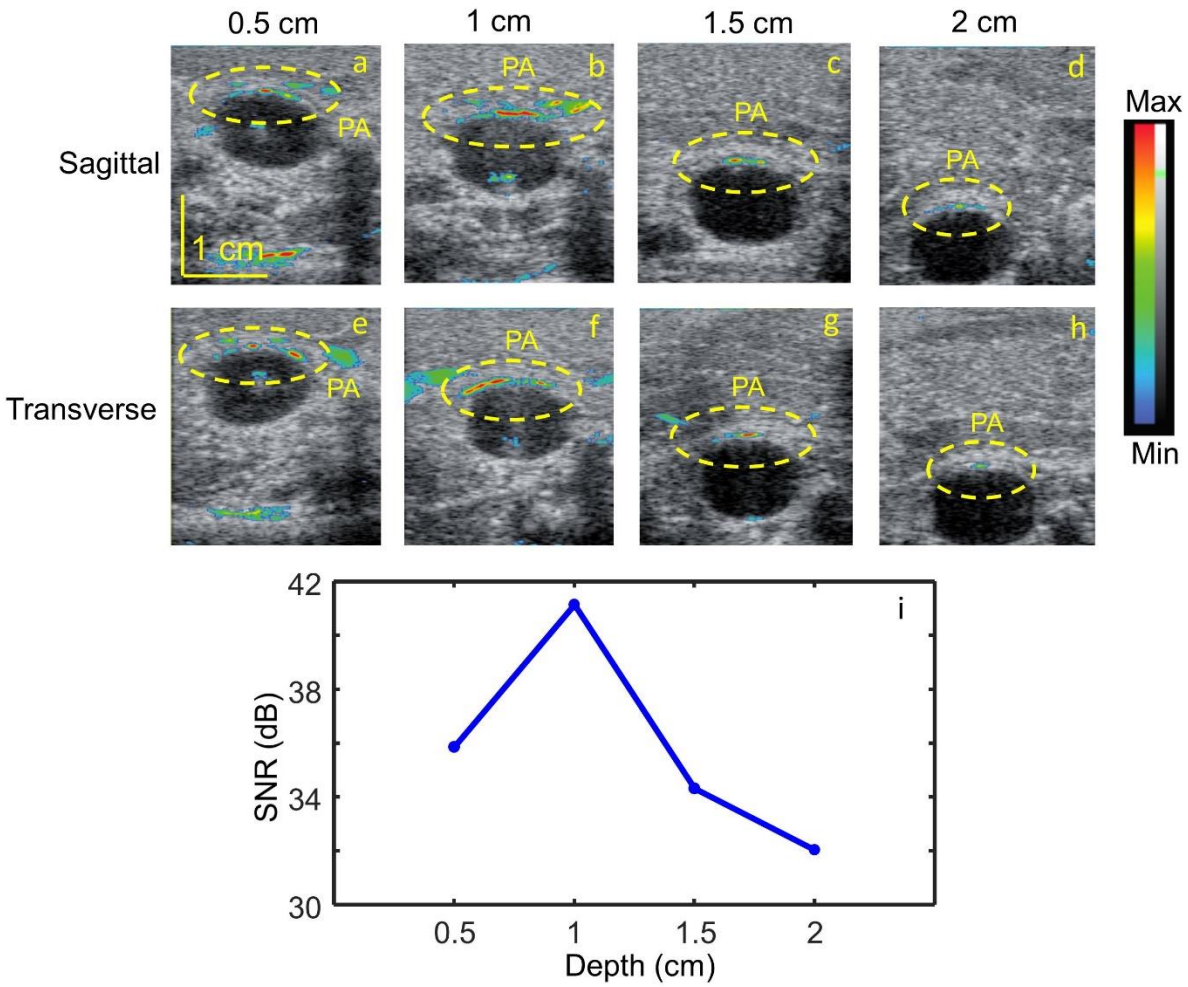

Figure 3. Depth imaging: (a-d) Combined US-PA images (sagittal plane) of the rat bladder at depths of 0.5 cm, 1 cm, 1.5 cm, and 2 cm, respectively. (e-h) Combined US-PA images (transverse plane) of the rat bladder at depths of 0.5 cm, 1 cm, 1.5 cm, and 2 cm, respectively. (i) Plot of SNR vs imaging depth.

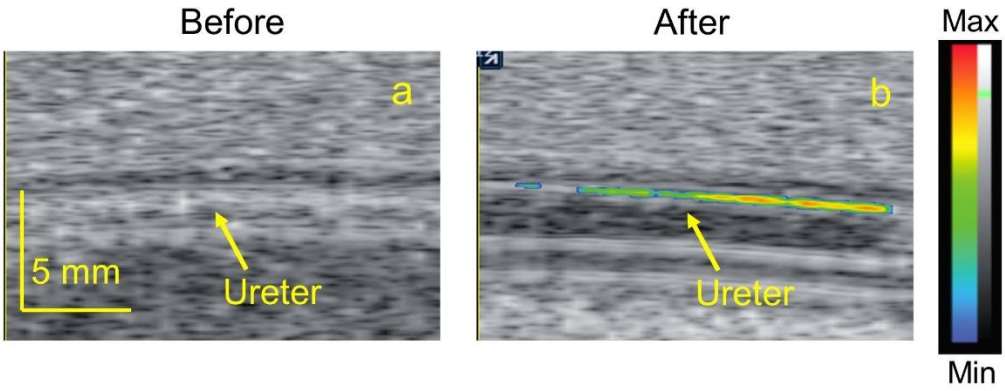

Figure 4. Vesicoureteral imaging: (a and b) Combined US-PA image of before and after the reverse flow of the black ink in the ureter mimicking phantom.

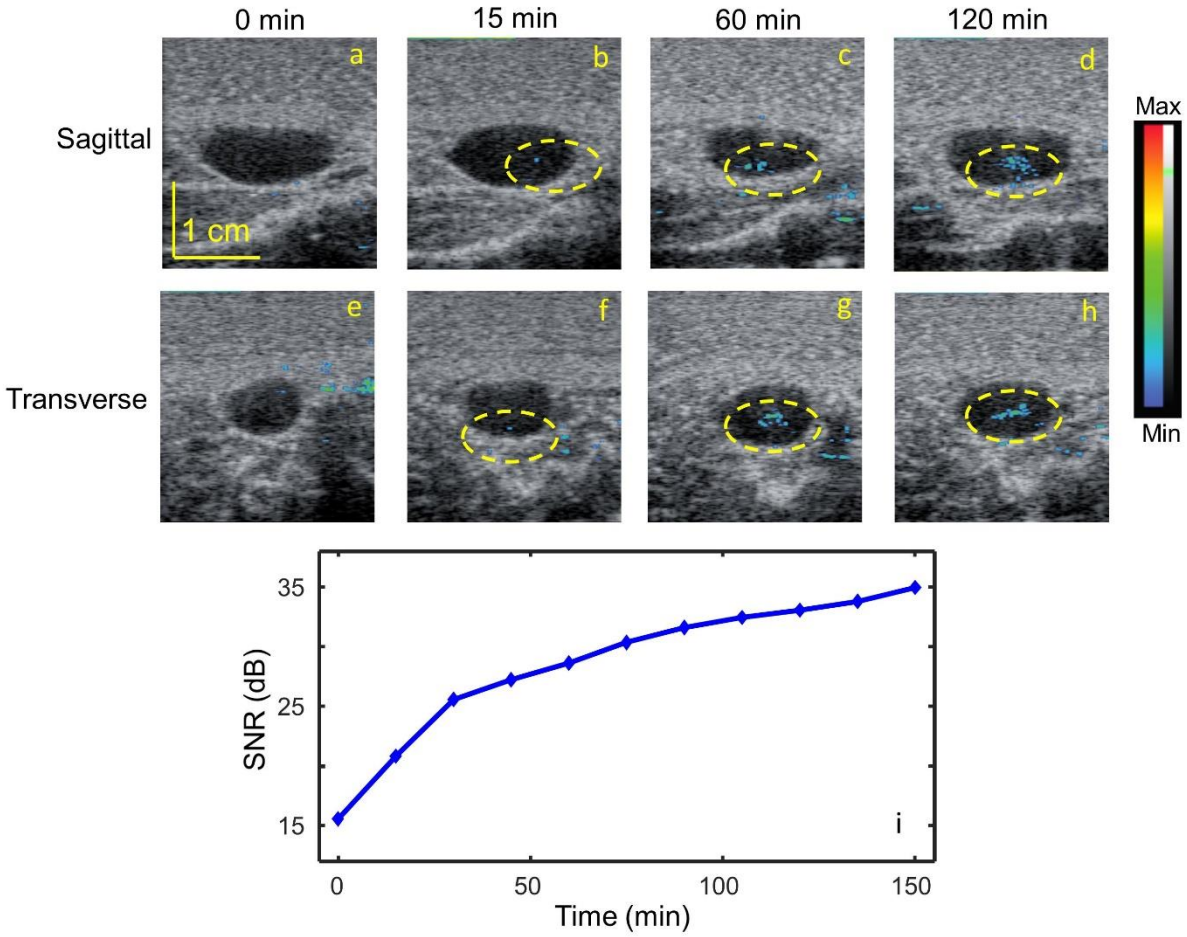

Figure 5. Nanoparticle clearance imaging: (a-d) Combined US-PA images of the bladder at 0 min, 15 min, 60 min, and 120 min, respectively, in the sagittal plane after tail vein injection of gold nanorods; (e-h) Combined US-PA images of the bladder at 0 min, 15 min, 60 min, and 120 min, respectively, in the transverse plane after tail vein injection of gold nanorods. (i) Plot showing SNR vs time of imaging (in minutes) after tail vein injection of gold nanorods.

Graphical Abstract

Non-invasive urinary bladder imaging is required for diagnosing various urinary tract infections and bladder cancer. Combined dual modal ultrasound-photoacoustic clinical imaging systems are being used for various biological applications. In this work photoacoustic imaging is used for structural and functional imaging of urinary bladder in rats. Structural imaging is demonstrated with black ink as contrast agent at 1064 nm. Imaging depth is up to 2 cm. Imaging of vesicoureteral reflux, a bladder disorder, is also shown in phantoms. Additionally, functional PA imaging, clearance of nanoparticles from circulation is also demonstrated by monitoring the accumulation of gold nanorods in the bladder.

TOC